JOURNAL OF CATALYSIS 130, 161–172 (1991)

Catalytic Behavior of Transition Metal Oxide in Graphite Gasification by Oxygen, Water, and Carbon Dioxide

Z. J. PAN AND R. T. YANG[1]

Department of Chemical Engineering, State University of New York at Buffalo, Buffalo, New York 14260

Received November 12, 1990; revised February 5, 1991

Vanadium oxide is used as a model transition metal-oxide catalyst for the gasification of graphite by O_2, H_2O, and CO_2. The following catalyst actions on the graphite basal plane are common in all three reactions: deep layer channeling, monolayer channeling, edge recession, and widening monolayer channeling. The steady-state oxidation states of vanadium in the reactions with CO_2 and H_2O are, respectively, V_3O_5 and V_2O_3 under the reaction conditions. The rate-limiting step in all channeling actions (for all three gasification reactions) is the oxidation on the surface of the metal oxide to increase the oxygen activity. Oxygen then diffuses through the nonstoichiometric metal-oxide particle to reach the carbon active sites where gasification takes place. (However, based on the channeling and TGA rate data, the catalyst surface oxidation is the rate-limiting step; the subsequent steps of diffusion of oxygen anion and C–C bond breakage steps are not rate-limiting.) This mechanism can explain the fact that transition metal oxides are the most active catalysts for the $C + O_2$ reaction but are only weakly active for the $C + H_2O$ and $C + CO_2$ reactions. The origin of the phenomenon of the widening monolayer channels is attributed to the anisotropy of the catalyzed reactivities of two adjacent zigzag edges of graphite.

INTRODUCTION

Much attention has been attracted to the behaviors and catalytic actions of catalysts (metals, metal oxides, and salts) in the gas–carbon reactions. The most important gas–carbon reactions involve O_2, CO_2, H_2O, or H_2 are the reactant. Although it has been known for many years that small amounts of catalysts can have dramatic effects on the rates of these reactions, which have been studied extensively (*1–3*), much of our present understanding of the catalytic behavior is attained from studies using microscopy. These studies have progressed from optical microscopy (*4*) to various techniques of electron microscopy, e.g., etch-decoration TEM (*5*) and controlled-atmosphere TEM (*6*).

A unique and most intriguing phenomenon associated with the catalyzed gas–graphite reactions is the motion of the catalyst on graphite which results in the catalytic activity. A number of catalyst motions (or actions) have been observed. The most extensively studied catalyst actions are pitting (*1, 7*), deep channeling (part of the extensive work by Baker has been reviewed in Refs. (*8, 9–14*), and deep edge recession (*13–16*). The two latter actions refer to the carving of channels and receding of line edges by the catalysts both of which involve many graphite layers, hence the term "deep" channeling. These two actions have been studied by using mainly controlled-atmosphere TEM.

The controlled-atmosphere TEM technique, however, relies on the relative contrast of images, which requires channels many graphite layers deep (e.g., >30 layers) and consequently "overlooks" catalytic events occurring on the surface layers of graphite. By using gold decoration, monolayer (single graphite layer) channeling and pitting by catalysts have been revealed and investigated in this laboratory (*17–21*). The

[1] To whom correspondence should be addressed.

0021-9517/91 $3.00

mechanistic steps involved in monolayer channeling in graphite hydrogenation by Group VIII metals and graphite oxidation by transition metal oxide are reasonably well understood (*17–21*). More important, the relative contribution to the total gasification rates by monolayer channeling is at least as important as that by deep channeling (*20*).

A most interesting problem concerning catalyzed carbon gasification is the contrast in the catalytic activities of transition metal oxides in different gas atmospheres, discussed in detail by Walker *et al.* (*2*) and Holstein and Boudart (*22*). Transition metal oxides are the most active catalysts for the $C + O_2$ reaction, but are only weakly active for the $C + CO_2$ and $C + H_2O$ reactions unless they are in reduced states (*2, 22*). This question is addressed in this work by a detailed comparison of the catalyst actions in the three atmospheres. In this study both deep channeling and monolayer surface phenomena were investigated in the atmospheres of H_2O and CO_2. V_2O_5 was chosen as the model transition metal oxide. The catalysis of the $C + O_2$ reaction by V_2O_5 has been studied extensively (*21, 23–25*). In the present study, the deep channeling phenomenon was examined without gold decoration, whereas the monolayer phenomena were studied by using gold decoration. No information on channeling in CO_2 is available because the controlled-atmosphere TEM technique is not suitable for CO_2 (*26*) due to interactions between CO_2 and the electron beam. This problem was avoided in the *ex situ* TEM technique employed in this study.

EXPERIMENTAL

Two types of graphite were used in this study. For the TEM study, the carbon used was a natural, single-crystal graphite from Ticonderoga, New York. This graphite was chosen for its well-defined crystalline structure and ability to be cleaved into specimens thin enough (700 to 1000 Å thickness) for TEM observation while maintaining a large single-crystal basal plane area. A detailed explanation of the techniques used to prepare the crystals for reaction, catalyst deposition, and subsequent gold decoration has been given elsewhere (*5, 27, 28*). For the TGA study, the graphite used was the SP-1 grade manufactured by the Carbon Products Division of Union Carbide Corp. The SP-1 graphite is a processed natural graphite containing less than 6 ppm impurities, in the form of flaky particles with a mean diameter of 30 μm and a thickness of 0.5 μm.

The catalysts were of puratronic grade, and powders of V, V_2O_3, and V_2O_5, all with purities well above 99.9%, were supplied by Alfa Products (Danvers, MA). The helium carrier gas was oxygen-free grade with a minimum purity of 99.995% and a maximum O_2 of 0.5 ppm. The CO_2 and O_2 had a minimum purity of 99.99%. The water vapor was generated by a gas wash bottle containing deionized–distilled water. Except when O_2 was used, these gases and mixtures were further purified by flowing through a column packed with copper turnings maintained at 550°C to remove the residual O_2.

The catalysts were deposited on the cleaved graphite from alcohol suspension for the TEM study. Before reactions, the samples were degassed in He at 500°C for 12 h. Other details of the TEM study were given elsewhere (*21*). The TGA measurements were conducted in a Cahn 2000 microbalance equipped with a quartz sample holder.

RESULTS AND DISCUSSION

Behavior of V_2O_5 on Graphite Basal Plane in Inert Atmosphere

After prolonged (12 h) heating at 500°C in He, particles of various faceted shapes were formed on the basal plane of graphite. The TEM picture of V_2O_5 on a thin graphite specimen after this heat treatment is shown a Fig. 1. Two general shapes of the particle were present: platelets and rod-shaped particles. The platelets were thin (as seen by the image contrast in TEM), whereas the rod-shaped particles were thicker.

The same V_2O_5/graphite specimen wa

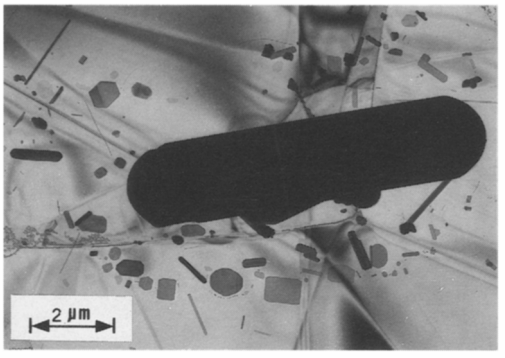

FIG. 1. TEM picture of V_2O_5 crystals on the basal plane of graphite after heating in He at 500°C for 12 h.

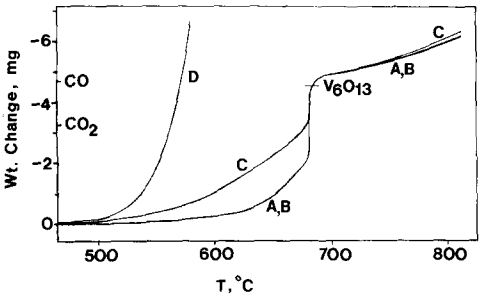

FIG. 3. TPR results of the reaction between V_2O_5 and graphite in different flowing gas atmospheres. The sample was a mixture of powders of 40 mg V_2O_5 and 80 mg SP-1 graphite. Heating rate = 1°C/min. (A) Dry He. (B) 10% CO_2 in He. (C) 3% H_2O in He. (D) 10% O_2 in He.

further heated rapidly (in 3 min) to 600°C in He and held at that temperature for 30 min. The TEM picture of the resulting specimen is shown as Fig. 2. (Prior to TEM observation, the specimens were quenched rapidly in He—the time allowed for cooling to 100°C was less than 1 min.) This specimen was subjected to gold decoration prior to TEM examination. The first result revealed by the TEM was the rapid disintegration and dispersion of the vanadium oxide into fine and less faceted particles. The more important result was the observation of the long etch pits (or channels) on graphite carved by the rod-shaped particles, as revealed by the decoration of the edges of the pits with gold nuclei. The pitting/channeling action was caused by the reaction between V_2O_5 and carbon in which V_2O_5 was reduced to a lower oxide. An XRD study by McKee (*23*) of the $V_2O_3 \rightarrow V_2O_5$ graphite mixture heated in N_2 (to 1100°C) indicated that the oxide was mainly V_6O_{13}. The TEM picture shown in Fig. 2 also revealed a liquid-like behavior of the vanadium oxide particles. The melting points of V_2O_5 and V_6O_{13} are 690 and 602°C, respectively, and are substantially higher for the lower oxides, e.g., 1967°C for V_2O_4, 1827°C for V_3O_5, 1970°C for V_2O_3, and 1890°C for V. From the above discussion, the reduced oxide shown in Fig. 2 was likely V_6O_{13}. The rapid dispersion of the particles upon heating to 600°C was the complex result of several physicochemical factors which have been discussed in detail by Ruckenstein (*29*).

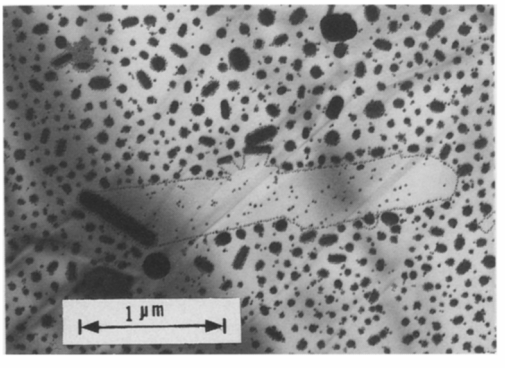

FIG. 2. TEM picture of V_2O_5 crystals on the basal plane of graphite after heating in He at 600°C for 30 min. The sample was decorated with fine gold nuclei (of 20–50 Å size).

TGA Study of V_2O_5—Graphite Reactions in Different Atmospheres

Figure 3 shows the results of temperature-programmed reaction of the V_2O_5–graphite mixture exposed to different atmospheres. The same weight loss rate was exhibited in both helium and 0.1 atm CO_2 atmospheres. This weight loss was caused by the reduction of V_2O_5 by carbon. A steep weight loss occurred at 680°C, which was near the melting points of V_2O_5 and V_6O_{13}, caused by the

wetting of V_2O_5/V_6O_{13} on the edges of the graphite crystals on which the active sites were located. A different weight loss rate was exhibited in 23-Torr water vapor (wet helium). Here the weight loss rate was significantly higher than in the case of helium and CO_2. However, the important result was that, as temperature was further increased beyond 680°C, the total weight loss (in H_2O) became nearly identical with the case of helium and CO_2. This result showed that the weight loss in water vapor at temperatures below 680°C was not due to gasification of carbon by water vapor, but was caused by an accelerated reduction of V_2O_5 by carbon. The function of water was as a catalyst in this reduction. Water is known to dissociate on vanadium oxides (*30, 31*). It is possible that part of the dissociated species oxidized carbon and the other part recombined with oxygen from bulk vanadium oxide to form water. Oxygen atoms in the nonstoichiometric vanadium oxides are both abundant and mobile (*32*).

The weight loss corresponding to the formation of V_6O_{13} (assuming CO was formed) is shown in Fig. 3. Continued weight loss beyond this point indicated that the vanadium oxide was in an oxide form lower than that of V_6O_{13}. The identification of these compounds is discussed later in this work.

The temperature-programmed results given in Fig. 3 show the initial interactions between V_2O_5 and graphite when exposed to different atmospheres. They do not give the steady-state catalyzed gas–carbon reaction rates. The steady-state carbon gasification rates were measured by TGA at fixed temperatures, as given in Table 1. These rates were obtained during the early stages of the reactions, after steady rates were approached. During this time, the catalyst was not V_2O_5. Increases in rates occurred during prolonged reactions because the graphite crystal sizes decreased, creating a higher active site density. It is seen from Table 1 that a nearly 10-fold increase in the rate of the C + O_2 reaction was caused by V_2O_5, and a much less, but still significant, increase took effect in the rates of gasification by CO_2 and H_2O.

TABLE 1

Steady-State Rates (in g/g/s) of Catalyzed and Uncatalyzed Gasification of SP-1 Graphite in Different Atmospheres

	Uncatalyzed	+2.8% (mol) V_2O_5
C + O_2 (0.2 atm), 600°C	2.88×10^{-5}	2.83×10^{-4}
C + H_2O (0.03 atm), 850°C	4.50×10^{-7}	6.31×10^{-7}
C + CO_2 (0.1 atm), 850°C	7.43×10^{-7}	9.19×10^{-7}

Modes of Catalyst Action in O_2, CO_2, and H_2O

The catalyst particles exhibit the same actions on the basal plane of graphite in O_2, CO_2, and H_2O. These common catalyst actions are summarized as follows. The deep channeling and deep edge recession, which have been discussed extensively in the literature except for the C–CO_2 reaction (8), originate from the deep steps of graphite. The monolayer channeling phenomenon has been studied for the C + H_2 (*18–20*) and C + O_2 (*21*) reactions and for the C + CO_2 and C + H_2O reactions in this work. Monolayer channeling originates from both vacancies and monolayer steps. The speed of monolayer channeling is far greater than that of deep channeling; the ratio of the speeds of monolayer/deep channelings is equal to the number of graphite layers in deep channeling. Thus the overall gasification rates by particles of the same size undergoing monolayer and deep channeling actions are equal (*18–21*). Without gold decoration, the high speed monolayer channeling action would appear to be a surface mobility phenomenon.

Another pervasive and significant catalysis action common in all three reactions (gasifications by O_2, CO_2, and H_2O) is the carving of monolayer channels by rod-shaped particles, which are being lengthened during the action. In the controlled-atmosphere TEM study of V_2O_5/graphite/O_2 by Baker *et al.*(*24*), these abundant, lengthening part

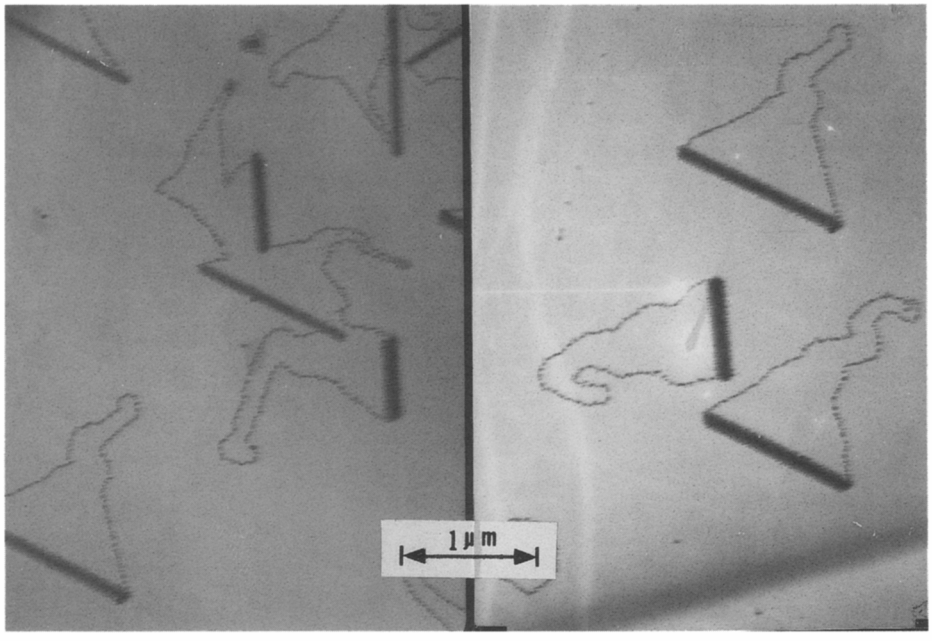

FIG. 4. TEM picture of V_2O_5 on graphite after reaction in 1 atm CO_2 at 600°C for 30 min followed by gold decoration. The zigzag directions of graphite (as marked) are determined by electron diffraction. The triangular (widening) channels are pervasive in reactions with O_2, H_2O, and CO_2.

cles were also observed and referred to as "lath" and "ribbon" formations. However, without gold decoration, again, the monolayer channels carved by these particles were not detectable in their work. Typical TEM pictures of the gold-decorated graphite with these rod-shaped particles are shown in Fig. 4. That the channels were monolayer in depth was verified by the same evidence as used in our previous monolayer channeling studies (*18*), i.e., the disappearance of the merging boundaries between these channels and monolayer etch pits, the rebounding of monolayer channeling particles at the boundaries of these channels, and the merging pattern between these channels (Fig. 4). A direct proof of the monolayer etch pits has been shown recently by scanning tunneling microscopy observation (*33*). The rod-shaped particles were oriented in specific directions. Electron diffraction results indicated that they were aligned only in the zigzag $(11\bar{2}0)$ direction of the graphite lattice. Such a preferred orientation was caused by the lower interfacial tension (and hence preferred wetting) between the vanadium oxide and the zigzag edge of graphite, as compared to that with the armchair edge. As the channeling proceeded and the particle was lengthened, the width of the particle did not apepar to decrease (seen in Both Fig. 4 and in Ref. (*24*)). The additional metal oxide was apparently gained in the same manner as in the Oswald ripening phenomenon of supported metal oxides (*29*).

As seen in Fig. 4, the particles initially underwent monolayer channeling action (maintaining the same channel width), but started to lengthen and widen the channel after a short period of time. As discussed later, many particles did not make such a change and continued the monolayer channeling action indefinitely. At this point, one needs to understand the origin of the widening action undertaken by certain particles (and the lack of it by other channeling particles).

Catalyzed monolayer edge recession pro-

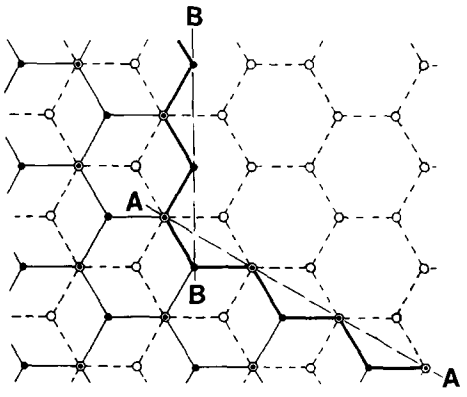

FIG. 5. Schematic representation of two graphite layers: the top layer by solid lines and dots, and the bottom layer by dashed lines and circles. AA and BB represent two adjacent zigzag edges of a hexagonal monolayer pit showing they are, in fact, different.

duced elongated hexagonal monolayer etch pits (*21*), which is another catalyst action common in all three reactions (by O_2, CO_2, and H_2O) catalyzed by meal oxides (as is also shown later in this work). The origin of the elongated hexagonal shape has been attributed to anisotropy of the reactivities on the adjacent zigzag edges of graphite, illustrated in Fig. 5 (also see Ref. (*21*)). In the V_2O_5/graphite system, these zigzag edges are coated or decorated by vanadium oxide. As shown in Fig. 5, it is not known which of the two adjacent edges (coated with vanadium oxide) is more reactive; the origin of the anisotropy is not understood. However, the ratio of the recession rates on these two faces (faces A and B in Fig. 5) has been determined to be 1.5 (*21*). Based on this anisotropy, it is possible to predict conditions under which the channeling particle will undergo the widening/lengthening mode of action. From our earlier electron diffraction results, there exist two types of crystallographic matching between the channeling particle and the graphite, as shown in Fig. 6 (*18*). For Case 1 in Fig. 6, if face A (the leading front face) is more active (by 1.5 times) than face B, the channel cannot widen because the fast forward movement does not allow widening. In contrast if face A is less active than face B, the recession on the two side faces is faster than the forward movement. Consequently, the channel widens and the particle becomes elongated. Moreover, since the ratio of the recession rates is 1.5 for B/A, the geometry of the triangular channel should preserve that ratio and take the shape such that the ratio of the side length over the height of the triangular channel is 1.5. This is approximately the case in Fig. 4. For Case 2 in Fig. 6, two leading front faces exist in the channel, one of which has a slower recession rate. For the same reason described above, the particle elongates along the slower receding face, and the channeling switches to the widening mode. The foregoing interpretation is also consistent with the fact that there exist more triangular channels than channels of constant widths.

Steady-State Channeling and Edge Recession for VO_x/Graphite/CO_2

The oxidation state of the VO_x particles was first to be determined. After a steady state was reached, the oxidation state of VO_X would no longer change. The steady-state oxidation state was determined by TGA and XRD. A mixture of V_2O_5/SP-1 graphite was reacted in a TGA reactor at 850°C and 1 atm CO_2. A steady state was reached after the rate of weight change reached a steady value. The sample was

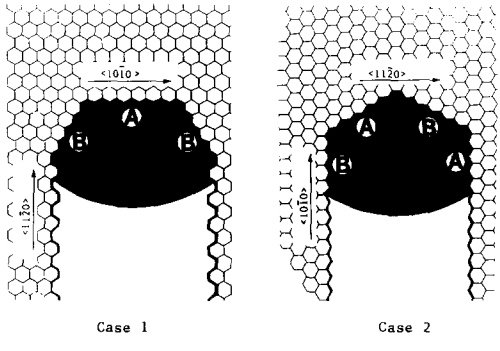

FIG. 6. Schematic representation of particles undergoing monolayer channeling on graphite in the armcha direction (Case 1) and zigzag direction (Case 2) (*18*)

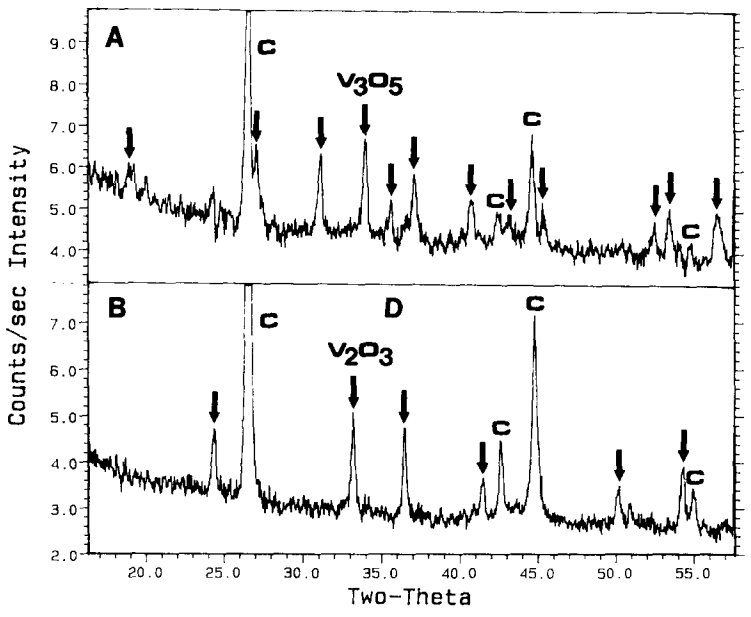

FIG. 7. XRD powder patterns (with Cu$K\alpha$) of reaction products after reaching steady-state. (A) VO_x/graphite/CO_2 (1 atm) at 850°C. (B) VO_x/graphite/H_2O (0.03 atm) at 850°C.

quenched rapidly in the CO_2 atmosphere (from 850 to 100°C within 1 min and at a slower rate to room temperature). In a separate experiment, a mixture of V/SP-1 graphite was subjected to the same procedure. The XRD powder patterns of these two treated samples were identical, as shown in Fig. 7A. Thus, the same steady-state oxidation state was reached regardless of the starting oxidation state of the VO_x. The XRD result showed only V_3O_5 (and graphite) with almost no other oxides present.

The same experiments were performed with 0.03 atm H_2O as the gaseous reactant, and the XRD pattern is shown in Fig. 7B, which was identical for both V and V_2O_5 as the starting catalyst. The XRD result indicated that the steady-state oxidation state in the VO_x/graphite/H_2O system at 850°C was V_2O_3. It should be noted that there exist at least 32 different XRD patterns (and structures) for vanadium oxides (see any XRD powder diffraction file). The steady-state VO_x studied in our systems (VO_x/C/CO_2 or H_2O) represents a thermodynamic equilibrium. Obviously, varying the temperature or the partial pressure of CO_2 or H_2O will change the VO_x structure and consequently its catalytic behavior for graphite gasification.

The catalyst channeling actions for the C + CO_2 reaction are summarized in Fig. 8. Figure 8 consists of TEM pictures of graphite samples after reaction with 1 atm CO_2 at 850°C. Since V_3O_5 (which was the steady-state oxide in this reaciton system) was not available, V_2O_3 was deposited on the graphite as the starting material, which should have rapidly converted to V_3O_5. Figure 8 reveals both deep and monolayer channeling actions. Deep channeling is shown in Figs. 8A and 8B. The speed of deep channeling was apparently inversely proportional to the depth of the channel as judged from the TEM image contrasts. For example, the channel depth in Fig. 8A was carved through the whole graphite sample, which was approximately 700–1000 Å thick. The channel depth in Fig. 8B was considerably shallower than the sample thickness, and the channeling speed was proportionally faster. Figure 8C reveals channels of the

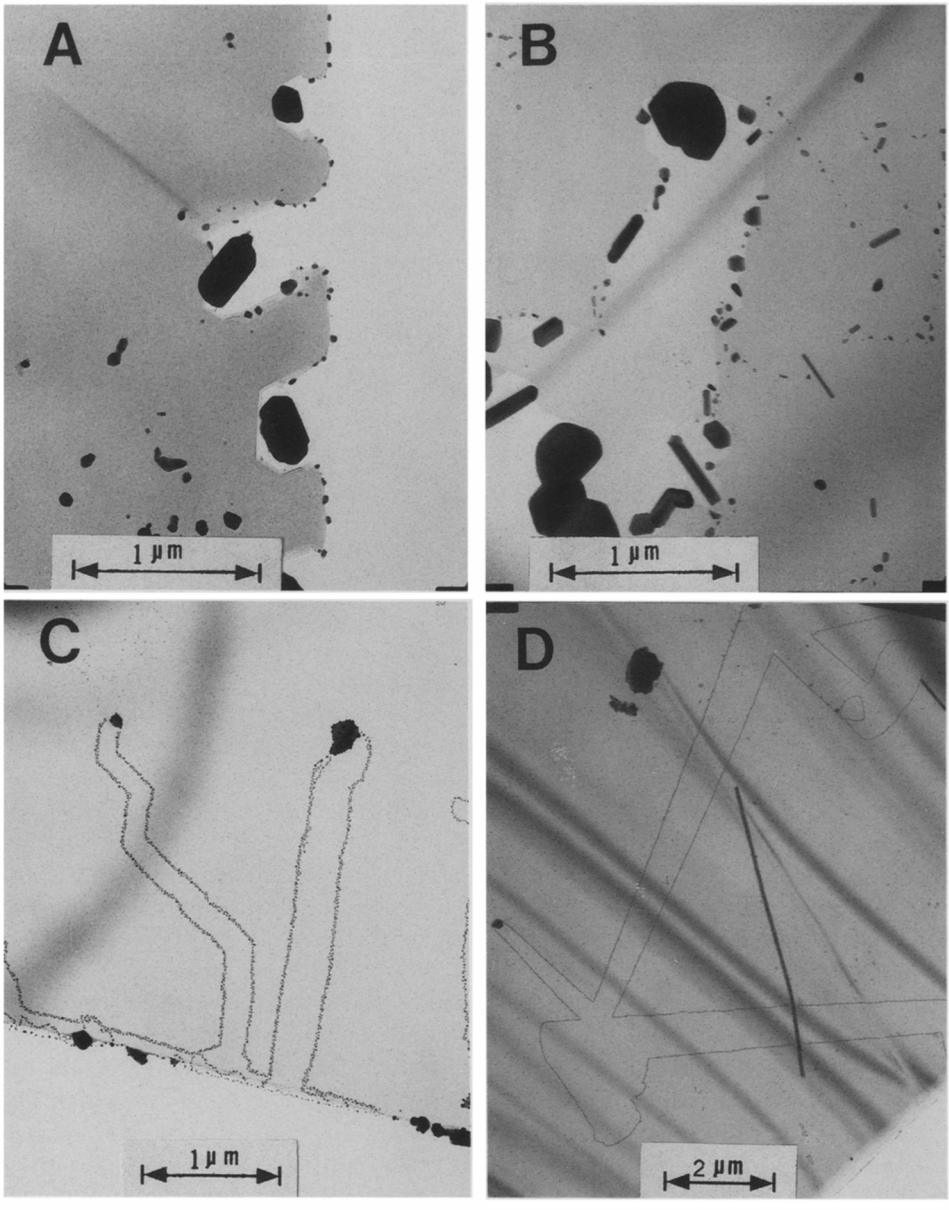

FIG. 8. TEM pictures of vanadium oxide on graphite after reaction with 1 atm CO_2 at 850°C for 2 h. A and B are without gold decoration; C and D are with gold decoration (note the double-line decoration).

depth of several graphite layers. The deep channels (in Figs. 8A, 8B, and 8C) all originated from steps or edges of the graphite. Monolayer channeling was much faster than the deep or multilayer channeling, and monolayer channels were more abundant than the deep channels. That these channels were indeed monolayer was verified in the same manner as described above and previously (*18*). The origins of the monolayer channels were vacancies and monolayer steps, both of which were abundant on cleaved graphite (*18*). Typical monolayer channels are shown in Fig. 8D.

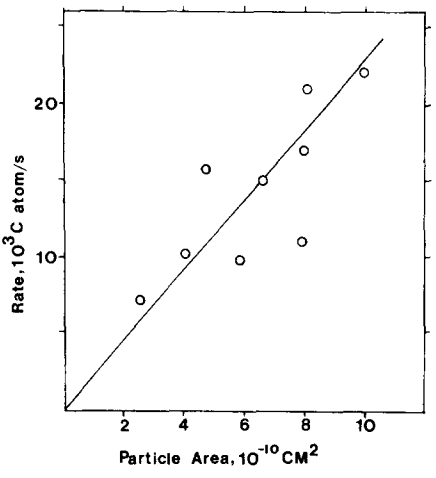

FIG. 9. Relationship between carbon gasification rate per particle of V_3O_5 and particle size (assuming hemispherical shape to calculate area) by monolayer channeling in 1 atm CO_2 at 850°C.

The monolayer channeling phenomenon has been examined on a large number of samples. It was found that the larger particles channeled at higher speeds, and that the channeling speed was actually proportional to the particle size. Figure 9 shows the dependence of the total carbon gasification rate per particle on the particle size. If the rate of carbon gasification was expressed based on per unit surface area of the V_3O_5 particle, this rate would be constant and is independent of the particle size. Based on the same analysis given previously for the $V_2O_5/C/O_2$ system (*21*), it was concluded that the rate-limiting step for the catalyzed C + CO_2 reaction was a reaction on the surface of the V_3O_5 particles. This was also the rate-limiting step in deep channeling, and the gasification rates by both deep and monolayer channeling were the same for the same particle size.

Going back to Fig. 8, it was also seen that the vanadium oxide wetted and decorated on the edges of the channels. Nuclei were formed on the edges of the deep channels (Figs. 8A and 8B). A thin film was formed on the edges of the shallower channels, as revealed by the double-line gold nuclei (Figs. 8C and 8D). The double-line gold nuclei were decorated on the two side edges of the vanadium oxide film (*21*). Since the higher oxides (V_2O_5 and V_6O_{13}) have low melting points, it is reasonable to assume that they were responsible for wetting on the edges.

The results described above lead to the conclusion that oxidation on the surface of the channeling particles by CO_2 was the rate-limiting step, for both monolayer and deep channeling. The oxidation step was between V_3O_5 and CO_2 to a higher oxidation state. Since the vanadium oxides (and all transition metal oxides) are highly nonstoichiometric (*32*) (for example, VO at 900°C exists in the range of $VO_{0.89-1.20}$), the mechanism of channeling must be discussed in that context (a rich discussion as given by Holstein and Boudart, (*22*)). The bulk of the channeling particle was V_3O_5. The surface was oxidized by CO_2 to increase the concentration or the activity of oxygen near the surface. The oxygen diffused (as interstitial ions or atoms) through bulk V_3O_5 (possibly through its anion vacancies) toward the V_3O_5/graphite interface, where it combined with the edge carbon atom to form CO/CO_2. The migration of the interstitial oxygen and the reaction with the edge carbon were much faster steps than the oxidation step (by CO_2). Dissociation of CO_2 was necessarily the first step in the oxidation.

Besides channels, monolayer elongated hexagonal etch pits were also observed in the C + CO_2 reaction (Fig. 10). The elongation was caused by anisotropy of reactivities of the adjacent zigzag edges. This phenomenon has been discussed in detail for the catalyzed C + O_2 reaction (*21*).

Steady-State Channeling and Edge Recession for VO_x/Graphite/H_2O

As mentioned above, the steady-state oxidation state of vanadium oxide in the C + H_2O reaction under the reaction conditions was V_2O_3. Particles of V_2O_3 were deposited on the graphite for reaction at 850°C in 0.03 atm H_2O for 4 h, followed by gold decora-

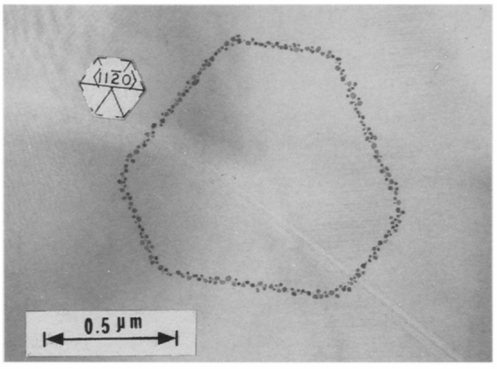

FIG. 10. TEM picture of gold-decorated monolayer etch pit formed by vanadium oxide on graphite basal plane in 1 atm CO_2 at 850°C for 2 h (note the double-line gold decoration).

tion/TEM studies. All characteristics of the catalyst behavior for this reaction were essentially the same as those in the C + CO_2 reaction. Figures 11A, 11B, and 11C show, respectively, deep channeling (700–1000 Å deep, initiated from the edge of graphite), multilayer channeling (initiated from a multilayer step), and monolayer channeling (initiated from lattice vacancies). The phenomenon of wetting by vanadium oxide was also seen.

The same dependence of channeling speed on channel depth was observed for this reaction (as that for the C + CO_2 reaction). For monolayer channeling, the same dependence of channeling speed on particle size was observed. Figure 12 depicts the relationship for monolayer channeling.

Clearly, the same mechanism for the catalyzed C + CO_2 reaction was followed in the C + H_2O reaction. The oxidation of the V_2O_3 particle on its surface by H_2O was the rate-limiting step for all channeling actions. The C + H_2O reactions catalyzed by KOH-transition metal oxides (*13*, *34*) and by $KCaO_x$ (*14*) were studied extensively. The major reaction products were H_2 and CO_2 (not CO). More important, it was found that H_2O dissociates on the catalyst to oxidize the catalyst (Ref. (*14*), p. 467) while producing H_2. This result is consistent with the above mechanism.

Comparison of TGA Rates of V_2O_3 Oxidation with Channeling Rates

Surface oxidation of the vanadium oxide is the rate-limiting step for both catalyzed C

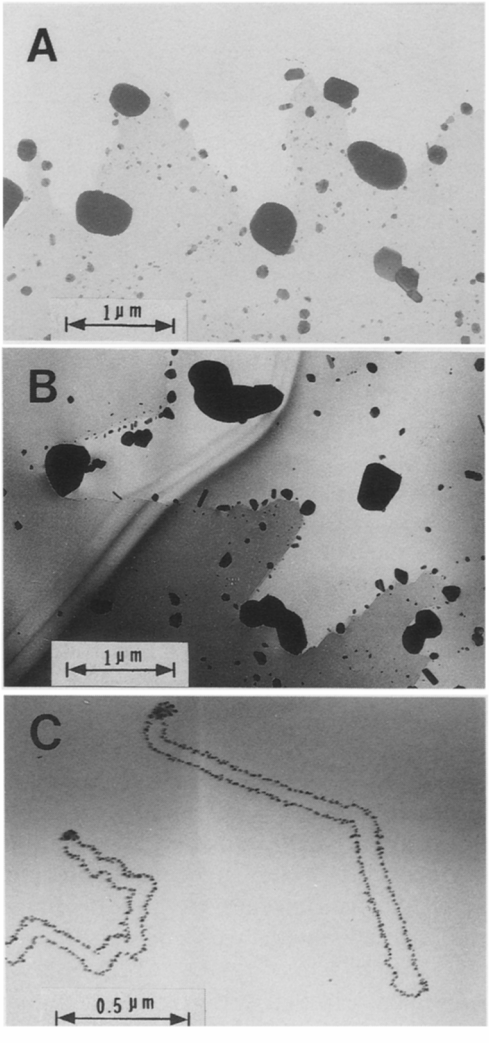

FIG. 11. TEM pictures of vanadium oxide on graphite after reaction with 0.03 atm H_2O at 850°C for 4 h. A and B are without gold decoration. C is with gold decoration.

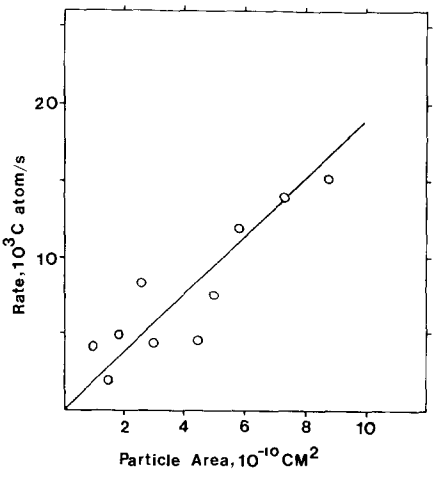

FIG. 12. Relationship between carbon gasification rate per particle of V_2O_3 and particle size (assuming hemispherical shape) by monolayer channeling in 0.03 atm H_2O at 850°C.

+ CO_2 and C + H_2O reactions. The catalyzed C + CO_2 reaction rate was equivalent to 2.3 × 10^{13} C atoms/s/cm^2 vanadium oxide, as calculated from Fig. 12. The equivalent rate for the C + H_2O reaction was 1.9 × 10^{13} C atoms/s/cm^2 vanadium oxide. Thus, the ratio for the two reaction rates was 1.2.

To provide further evidence for the surface oxidation limited mechanism, TGA rates for the oxidation of vanadium oxide were measured. Powder of V_2O_3 (sizes less than 325 mesh) was used. Steady-state oxidation rates of the powder were measured at 850°C, separately, in 1 atm CO_2 and 0.03 atm H_2O. The resulting powder from both reactions was analyzed by XRD, and V_2O_4 was identified in both cases. Assuming the V_2O_3 powder had an average particle diameter of 10 μm, the oxidation rate (TGA) in 1 atm CO_2 was 2.1 × 10^{13} O atoms/s/cm^2 V_2O_3. The TGA rate in 0.03 atm H_2O was 1.7 × 10^{13} O atms/s/cm^2 V_2O_3. These values compared favorably with the values calculated from the catalyst channeling rates. The relative oxidation rates in the two gases (a ratio of 1.2) also agreed with the relative channeling rates. This result is indeed a satisfactory support of the catalyzed reaction mechanism discussed above.

Finally, the relative catalytic activities of vanadium oxide in the three carbon gasification reactions (by O_2, H_2O, and CO_2) should be discussed. The surface oxidation of vanadium oxide to a higher oxidation state is the rate-limiting step for all three reactions ((*21*) and this work). The oxygen diffuses through the vanadium-oxide catalyst to the catalyst–graphite interface, where the graphite edge atom (with a free sp^2 electron) is the active site capable of reaction with the oxygen atom to form CO or CO_2. Therefore, the catalyst activity depends on the ability of the gas to oxidize the vanadium oxide, and this appears to be the reason that vanadium oxide is a most effective catalyst for the C + O_2 reaction but is only weakly effective for the reactions with CO_2 and H_2O. Another factor in determining the catalyst activity is its ability to wet and spread on graphite to cover the edge carbon active sites. In the O_2 atmosphere, transition metals at higher oxidation states are formed which generally have lower melting points and hence spread and disperse better. This is an additional reason for the high activities of transition metal oxides in the C + O_2 reaction similar to the CaO-catalyzed C + O_2 reaction, where a direct correlation between the rate and the surface area of the dispersed CaO has been observed (the reaction system follows a similar redox mechanism) (*35*).

ACKNOWLEDGMENTS

This work was supported by the National Science Foundation under Grant CBT-8703677.

REFERENCES

1. Walker, P. L., Jr., Rusinko, F., Jr., and Austin, L. G., in "Advances in Catalysis" (D. D. Eley, P. W. Selwood, and P. B. Weisz, Eds.), Vol. 11, p. 133. Academic Press, New York, 1959.
2. Walker, P. L., Jr., Shelef, M., and Anderson, R. A., *in* "Chemistry and Physics of Carbon" (P. L. Walker, Ed.). Dekker, New York, 1968).
3. Figuereido, J. L., and Moulijn, J. A., *in* "Carbon

and Coal Gasification—Science and Technology" (J. L. Figuereido and J. A. Moulijn, Eds.). NATO ASI Series E, No. 105, Nighoff, The Hague, 1986.
4. Hennig, G. R., *Proc. Conf. Carbon 1st 2nd*, 112 (1956).
5. Hennig, G. R., *in* "Chemistry and Physics of Carbon" (P. L. Walker, Jr., Ed.), Vol. 2. Dekker, New York, 1966.
6. Baker, R. T. K., *Catal. Rev. Sci. Eng.* **19(2),** 161 (1979).
7. Thomas, J. M., *in* "Chemistry and Physics of Carbon" (P. L. Walker, Jr., Ed.), Vol. 1. Dekker, New York, 1965.
8. Baker, R. T. K., *in* "Carbon and Coal Gasification—Science and Technology" (J. L. Figuereido and J. A. Moulijn, Eds.), NATO ASI Series E, No. 105, p. 231, Nijhoff, The Hague, 1986.
9. Hennig, G. R., *J. Inorg. Nucl. Chem.* **24,** 1129 (1962).
10. McKee, D. W., *in* "Chemistry and Physics of Carbon" (P. L. Walker, Jr., and P. A. Thrower, Eds.), Vol. 16. Dekker, New York, 1980.
11. Keep, C. W., Terry, S., and Wells, M., *J. Catal.* **66,** 451 (1980).
12. Coates, D. J., Evans, J. W., Cabrera, A. L., Somorjai, G. A., and Heinemann, H., *J. Catal.* **80,** 215 (1983).
13. Carrazza, J., Chludzinski, J. J., Heinemann, H., Somorjai, G. A., and R. T. K. Baker, *J. Catal.* **110,** 74 (1988).
14. Pereira, P., Csencsits, R., Somorjai, G. A., and Heinemann, H., *J. Catal.* **123,** 463 (1990).
15. Harris, P. S., Feates, F. S., and Reuben, B. G., *Carbon* **11,** 565 (1973).
16. Baker, R. T. K., *Carbon* **24,** 715 (1986).
17. Yang, R. T., and Wong, C., *J. Catal.* **85,** 154 (1984).
18. Goethel, P. J., and Yang, R. T., *J. Catal.* **101,** 342 (1986).
19. Goethel, P. J., and Yang, R. T., *J. Catal.* **108,** 356 (1987).
20. Goethel, P. J., and Yang, R. T., *J. Catal.* **111,** 220 (1988).
21. Goethel, P. J., and Yang, R. T., *J. Catal.* **119,** 201 (1989).
22. Holstein, W. L., and Boudart, M., *Fuel* **62,** 162 (1983).
23. McKee, D. W., *Carbon* **8,** 623 (1970).
24. Baker, R. T. K., Thomas, R. B., and Wells, M., *Carbon* **13,** 141 (1975).
25. Moreno-Castilla, C., Rivera-Utrilla, J., and Lopez-Peinado, A., *Fuel* **68,** 968 (1989).
26. Baker, R. T. K., Lund, C. R. F., and Chludzinski, J. J., *J. Catal.* **87,** 255 (1984).
27. Wong, C., Ph.D. dissertation, State University of New York at Buffalo, Buffalo, NY, 1983.
28. Yang, R. T., *in* "Chemistry and Physics of Carbon" (P. A. Thrower, Ed.), Vol. 19. Dekker, New York, 1984.
29. Ruckenstein, E., *in* "Metal-Support Interactions in Catalysis, Sintering and Redispersion" (S. A. Stevenson, J. A. Dumesic, R. T. K. Baker, and E. Ruckeinstein, Eds.), pp. 141–308. Van Nostrand–Reinhold, New York, 1987.
30. Kurtz, R. L., and Henrich, V. E., *Phys. Rev. B* **28,** 6699 (1983).
31. Kung, H. H., "Transition Metal Oxides: Surface Chemistry and Catalysis," Chap. 6. Elsevier, New York, 1989.
32. Sorensen, O. T., Eds., "Nonstoichiometric Oxides," Chaps. 1 and 8. Academic Press, New York, 1981.
33. Chang, H., and Bard, A. J., *J. Am. Chem. Soc.* **112,** 4598 (1990).
34. Carrazza, J., Tysoe, W. T., Heinemann, H., and Somorjai, G. A., *J. Catal.* **96,** 234 (1985).
35. Radovic, L. R., Walker, P. L., Jr., and Jenkins, R. G., *J. Catal.* **82,** 382 (1983).